Interplay of Darrieus-Landau instability and weak turbulence in premixed flame propagation

Francesco Creta,* Rachele Lamioni, and Pasquale Eduardo Lapenna
Department of Mechanical and Aerospace Engineering, University of Rome La Sapienza, Rome, Italy

Guido Troiani
ENEA C.R. Casaccia, via Anguillarese 301, Rome, Italy

(Received 5 August 2016; revised manuscript received 28 September 2016; published 3 November 2016)

In this study we investigate, both numerically and experimentally, the interplay between the intrinsic Darrieus-Landau (DL) or hydrodynamic instability of a premixed flame and the moderately turbulent flow field in which the flame propagates. The objective is threefold: to establish, unambiguously, through a suitably defined marker, the presence or absence of DL-induced effects on the turbulent flame, to quantify the DL effects on the flame propagation and morphology and, finally, to asses whether such effects are mitigated or suppressed as the turbulence intensity is increased. The numerical simulations are based on a deficient reactant model which lends itself to a wealth of results from asymptotic theory, such as the determination of stability limits. The skewness of the flame curvature probability density function is identified as an unambiguous morphological marker for the presence or absence of DL effects in a turbulent environment. In addition, the turbulent propagation speed is shown to exhibit a distinct dual behavior whereby it is noticeably enhanced in the presence of DL instability while it is unchanged otherwise. Furthermore, increasing the turbulence intensity is found to be mitigating with respect to DL-induced effects such as the mentioned dual behavior which disappears at higher intensities. Experimental propane and/or air Bunsen flames are also investigated, utilizing two distinct diameters, respectively, above and below the estimated DL cutoff wavelength. Curvature skewness is still clearly observed to act as a marker for DL instability while the turbulent propagation speed is concurrently enhanced in the presence of the instability.

DOI: 10.1103/PhysRevE.94.053102

I. INTRODUCTION

Since the seminal work of Darrieus [1] and Landau [2], the planar configuration of a premixed flame (a deflagrating front), propagating at constant speed with respect to the fresh combustible mixture, was observed to exhibit instability with respect to perturbations of any wave number. The effect, referred to as Darrieus-Landau (DL) or hydrodynamic instability, was recognized to be caused by the flow expansion and the ensuing streamline coalescence or deviation in the presence of small flame perturbations, leading to local flow acceleration or deceleration and relative amplification of the flame wrinkling. Markstein [3] later introduced a phenomenological dependence of flame speed on flame curvature, conditioning the instability to small wave numbers alone. More rigorous asymptotic theories subsequently appeared, based on the multi-scale structure of premixed flames [4], eventually deriving a hydrodynamic model [5] from which emerged a linear dependence of flame speed on stretch rate, which incorporates both curvature as well as hydrodynamic strain effects, both modulated by a parameter known as Markstein length, of the order of flame thickness, representative of diffusive effects. As a result, the operating pressure, mixture composition, and type, which all affect the Markstein length, are parameters which are expected to affect the cutoff wave number of the DL instability [6]. Clearly, the larger the characteristic hydrodynamic length, established by the geometrical features of the experimental apparatus (or computational domain), with respect to the cutoff wavelength, the more intense the DL instability.

A considerable number of experiments revealed DL instabilities in a variety of premixed flame configurations in the form of flame surface corrugation [7–9]. In particular, the laminar propagation of spherical flames revealed self-acceleration due to the onset of a fractal conformation, brought about by DL instability as the flame expands [10,11]. The emergence of fractal flame structures was also observed using a variety of numerical models, ranging from weakly nonlinear Sivashinksky-like models [12,13] to large scale fluid dynamic computations [14].

Of particular importance, albeit utilizing different standpoints, is the observation that DL effects may play a considerable role not merely in a laminar setting but also in the context of turbulent propagation of premixed flames [15–19]. Indeed, a number of experimental studies were carried out emphasizing the specific role of intrinsic DL instability [20–23] in premixed turbulent flame propagation. However, the interplay between DL-induced corrugation and turbulence-induced wrinkling and the manner in which they act synergistically to augment the turbulent propagation speed is still a matter of intense scrutiny (a critical review of instability effects in turbulent combustion can be found in [24]). In particular, the well-known difficulty in determining a universal scaling law for the turbulent propagation speed in terms of the operative parameters, a task generally hindered by the strong dependence from experimental conditions, can be subject to an additional layer of complexity in the presence of DL instability. An inherent problem in experiments, for example, is the absence of a reliable criterion to determine the presence of DL instability. In spite of this, recent numerical and theoretical work [25–27] strongly suggest a potentially significant influence of DL effects on turbulent propagation, especially at lower turbulence intensity.

*francesco.creta@uniroma1.it

If we are to attempt to distill open issues from the experiments dedicated to the analysis of DL effects on turbulent propagation, three distinct questions would arise, namely: (i) unambiguously establish the presence or absence of a DL-induced flame morphology on a turbulent premixed flame, given the operating conditions and the fuel type, (ii) quantify the effect of the intensity of the DL instability on the flame morphology and propagation, and (iii) investigate whether the DL-induced effects are mitigated or even suppressed as the intensity of the turbulence increases.

In this work we address the above questions utilizing first a series of large scale numerical simulations of two-dimensional, slot burner, premixed turbulent flames, a configuration which allows the attainment of statistical steadiness of any derived flame property. We identify the stability limits for the flame in such a way as to induce or suppress DL instability at will. We then identify the skewness of the flame curvature distribution as a statistical morphological quantity to be used as an unambiguous marker for DL-induced effects on the turbulent flame. We also measure the turbulent propagation speed and assess the effect of the intensity of the DL instability and of the incident turbulence. Secondly we perform a series of experiments on propane-air, atmospheric pressure Bunsen flames at different equivalence ratios and different Reynolds numbers. We utilize two distinct Bunsen diameters which are chosen to be respectively above and below the estimated cutoff wavelength in the range of compositions used. The previously defined morphological marker is successfully validated on the experimental flames, proving it can be used to identify the presence of DL effects on turbulent flames.

II. NUMERICAL SIMULATIONS

To study the morphological properties of premixed flames subject to DL instability, we adopt a one-step irreversible Arrhenius reaction model in which a deficient reactant determines the reaction rate and is entirely depleted across the flame while the concentration of other reactants remains essentially unchanged. We further assume low-Mach number conditions which are justified as a deflagration wave propagates at a speed S_L^0 (unstretched laminar flame speed) far smaller than the speed of sound in the combustible mixture. We note that the use of the deficient reactant model enables the coherent use of results obtained within the asymptotic hydrodynamic theory of premixed flames developed in Ref. [5] and in particular the linear stability properties of flames derived therein.

We nondimensionalize spatial variables with respect to a hydrodynamic length scale L, which is assumed as the width of the slot burner, while time is nondimensionalized by L/S_L^0. Other nondimensional variables, such as density and mass fraction of the deficient reactant, are measured in units of ρ_u and Y_u, where the subscript 'u' denotes the value in the unburned fresh mixture, while velocities are measured in units of S_L^0. The nondimensional temperature is defined as $\theta = (T - T_u)/(T_{ad} - T_u)$, where T is the dimensional temperature and T_{ad} is the adiabatic flame temperature, i.e., the temperature downstream of an adiabatic unstretched planar flame. Associated to the flame is a diffusive length scale $\ell_D = \lambda/\rho_u c_p S_L^0 = \mathcal{D}_{th}/S_L^0$, where λ and c_p are the thermal conductivity and specific heat at constant pressure of the combustible mixture, respectively, and $\mathcal{D}_{th}$ the thermal diffusivity. The ensuing conservation equations thus read

$$\rho\left(\frac{\partial u_i}{\partial t} + \frac{\partial}{\partial x_j}(u_i u_j)\right) = \frac{\partial}{\partial x_j}\left(-p_1\delta_{ij} + \frac{1}{\mathrm{Re}}S_{ij}\right), \quad (1)$$

$$\rho\left(\frac{\partial Y}{\partial t} + u_j\frac{\partial Y}{\partial x_j}\right) = \frac{\delta}{\mathrm{Le}}\frac{\partial}{\partial x_j}\frac{\partial Y}{\partial x_j} - \frac{\Omega}{\delta}, \quad (2)$$

$$\rho\left(\frac{\partial \theta}{\partial t} + u_j\frac{\partial \theta}{\partial x_j}\right) = \delta\frac{\partial}{\partial x_j}\frac{\partial \theta}{\partial x_j} + \frac{\Omega}{\delta}, \quad (3)$$

where $\delta = \ell_D/L$ is the nondimensional diffusive length which is taken as a measure of the flame thickness. $\mathrm{Le} = \lambda/c_p\mathcal{D}$ is the Lewis number measuring the ratio of the heat to mass diffusivity, with $\mathcal{D} = \rho_u D$, where D is the diffusion coefficient of the deficient reactant. $\mathrm{Re} = \rho_u S_L^0 L/\mu$ is the Reynolds number, with μ the dynamic viscosity, and the effect of buoyancy is neglected. Dynamic viscosity μ, thermal conductivity λ, specific heat c_p, and coefficient $\mathcal{D}$ are assumed constant. The viscous stress tensor reads

$$S_{ij} = \frac{\partial u_i}{\partial x_j} + \frac{\partial u_j}{\partial x_i} - \frac{2}{3}\delta_{ij}\frac{\partial u_k}{\partial x_k}. \quad (4)$$

Under the low-Mach assumption the dimensional hydrodynamic pressure P_1 (where its nondimensional counterpart is $p_1 = P_1/\rho_u {S_L^0}^2$) represents an $O(M^2)$ deviation, with $M \ll 1$ being the Mach number, from the thermodynamic pressure P_0 which is uniform in space. Thus the equation of state for a perfect gas mixture once nondimensionalized reads $\rho = (\theta(\sigma - 1) + 1)^{-1}$, where $\sigma = T_{ad}/T_u$ is the ratio of the adiabatic flame temperature to the unburned mixture temperature. The continuity equation reduces to a constraint on the divergence of the velocity as follows

$$\frac{\partial u_j}{\partial x_j} = -\frac{1}{\rho}\left(\frac{\partial \rho}{\partial t} + u_j\frac{\partial \rho}{\partial x_j}\right) = (\sigma - 1)\left(\delta\frac{\partial}{\partial x_j}\frac{\partial \theta}{\partial x_j} - \frac{\Omega}{\delta}\right). \quad (5)$$

Finally, the reaction rate takes the form

$$\Omega = \frac{\mathrm{Ze}^2}{2\mathrm{Le}}\,Y\,\exp\left(\frac{\mathrm{Ze}(\theta - 1)}{1 + \alpha(\theta - 1)}\right), \quad (6)$$

where $\mathrm{Ze} = T_a(T_{ad} - T_u)/T_{ad}^2$ is the Zel'dovich number, with $T_a = E_a/\mathcal{R}$ the activation temperature and E_a activation energy and $\alpha = 1 - \sigma^{-1}$.

The spatial discretization of the governing equations is based on the spectral element method [28,29] which splits the computational domain into E conforming rectangular elements. In each of the spectral elements, the solution is approximated by an $N - 1$ dimensional tensor-product based on the Nth order Lagrange polynomials which are defined on Gauss-Lobatto-Legendre quadrature points. The discretized system of equations is solved numerically using a modified version of the highly scalable, incompressible, and low-Mach number spectral element flow solver NEK5000 [30]. Time integration is performed using a high-order splitting scheme for the low-Mach number variable density flows [31] decoupling the stiff thermochemistry subsystem (temperature and deficient reactant equations) from the hydrodynamic

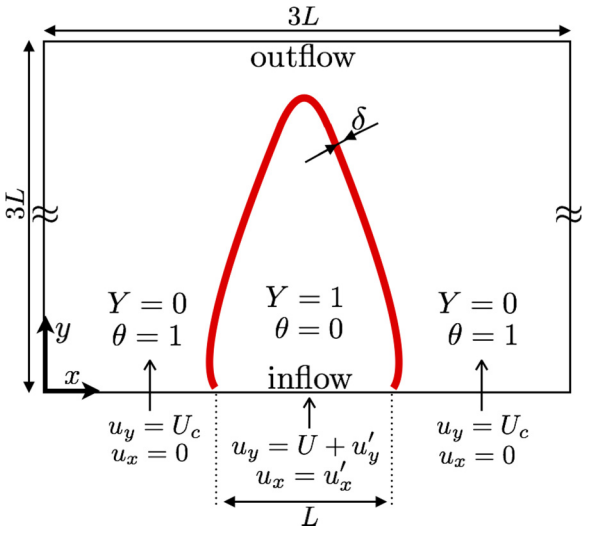

FIG. 1. Schematic of the computational domain.

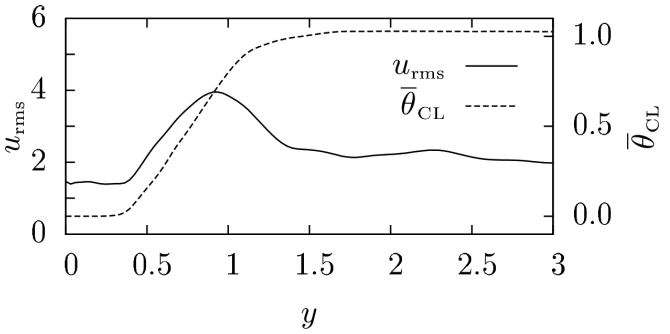

FIG. 2. Root mean square of velocity perturbations $u_{\rm rms}$ (solid line) and mean temperature $\overline{\theta}_{\rm CL}$ (dashed line) along the slot centerline for $\delta = 0.008 < \delta_c$ and $u'_0 = 1.5$.

subsystem (momentum equation). The thermochemistry subsystem is integrated by means of the stiff ordinary differential equation solver CVODE [32], while the hydrodynamic subsystem is advanced in time using a third-order semi-implicit formulation [29,33,34].

Numerical simulations are performed on a two-dimensional rectangular domain of non-dimensional width $L_x/L = 3$ and height $L_y/L = 3$, where, again, L is the width of the slot burner, taken to be the reference hydrodynamic length and placed symmetrically at the lower boundary. The order N of each element is chosen so as to guarantee a minimum of ten grid points within the flame thickness δ, with the exception of the minimum simulated flame thickness $\delta = 0.004$. The latter required the highest resolution with $E = 512$ and $N = 8$ for each spatial dimension resulting in ≈6 points within the flame thickness.

Free-slip boundary conditions for the velocity and zero-flux for the scalars (temperature and deficient reactant) are adopted at the left and right boundaries of the computational domain, while zero-flux outflow conditions for both scalars and velocity components are used at upper boundary. Inflow conditions for both velocity and scalars are used at the lower boundary. A representation of the computational domain is displayed in Fig. 1. In particular at the slot burner inflow, Dirichlet conditions for temperature and deficient reactant are imposed, $\theta = 0$ and $Y = 1$, corresponding to a fresh mixture with nondimensional bulk inflow velocity $u_y = U = 3$. The latter velocity, in laminar conditions, corresponds to a slot flame height which approximately extends half the height of the domain. A laminar coflow condition at the lower boundary on each side of the burner inflow is also implemented, with $\theta = 1$ and $Y = 0$, corresponding to a burned mixture so as to stabilize the slot flame. The vertical coflow velocity magnitude $u_y = U_c$ is set at a value of the same order of the velocity magnitude downstream of the laminar slot flame (e.g., for $\sigma = 8$, $U_c \approx 8$) so as to minimize shear and avoid Kelvin-Helmholtz instabilities interfering with the dynamical features of the flame.

Superimposed to the burner bulk inflow, a homogeneous, isotropic, synthetic turbulence signal is added possessing prescribed two-point statistics. In particular, the velocity perturbation signals $u'_i(x,y)$, generated using a method developed by Klein [35] and illustrated in [13], possess a prescribed autocorrelation function $R_{uu}(r) = \exp(-\pi r^2/4\ell^2)$, with r the distance between two points [36], which give them a spatial scale ℓ resembling an integral scale, in addition to an intensity $u'_0 = \overline{(u'_i u'_i)}^{1/2}$ which is taken as representative of the intensity of the fluctuating flow-field impacting the flame. The inflow perturbation velocities $u'_i(x,t)$ are simply obtained by sweeping the signals $u'_i(x,y)$ with $y = Ut$. Note that the Reynolds number was kept constant (Re = 200) for all simulations in order to maintain the same degree of viscous dissipation leading to identical decay rates of the inflow turbulence. As shown in Fig. 2 for a representative case ($\delta = 0.008$, $u'_0 = 1.5$), the rms of the velocity perturbations along the slot burner centerline exhibits an approximate decay of 10% at a vertical distance of $y = 0.5$ from the burner inlet, which can be assumed as the position of the flame brush leading edge where the flame brush region can be inferred from the mean temperature profile along the centerline. Note the increase in rms corresponding to the flame brush region, caused by the effect of flame tilt and thermal expansion [26].

Table I displays all the operative parameters used in the numerical simulations, a selection of which is visible in Fig. 3. The flame thickness δ acts as a bifurcation parameter, suppressing DL instability above a critical value δ_c and promoting them below such value. The determination of δ_c is illustrated below. The Lewis number, on the other hand, was kept above unity to suppress any thermal diffusive instability. For the other parameters listed in Table I, representative values for common hydrocarbon fuels are assumed. Given the range of ℓ/δ and u'_0 used, the regime spanned by the simulations is that of 'corrugated flamelets', extending up

TABLE I. Main parameters used in the numerical simulations of two-dimensional slot burner flames.

δ	σ	Le	Ze	u'_0	ℓ
0.004–0.05	8	1.2	9	1.5,2.5	0.05

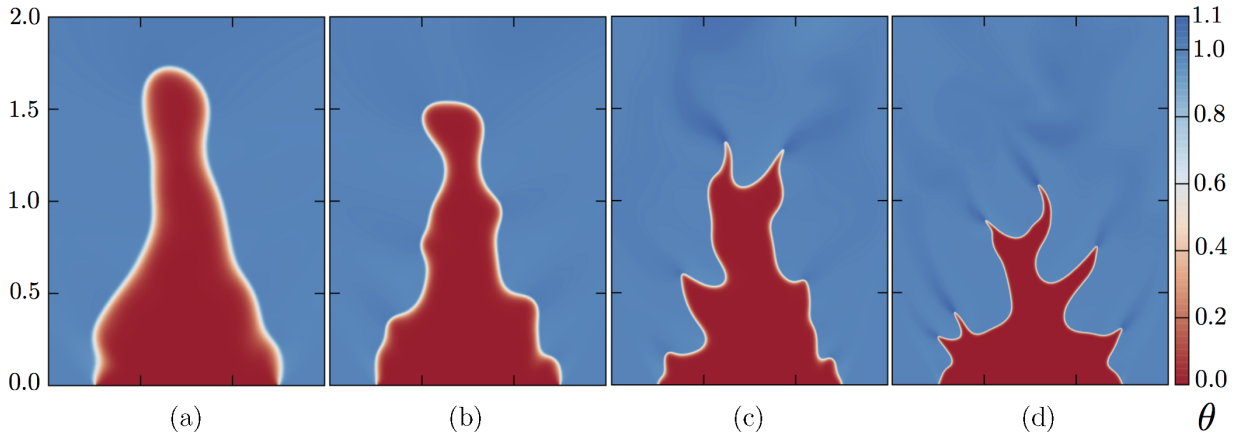

FIG. 3. Two-dimensional simulations of slot burner flames with $\sigma = 8$, Le $= 1.2$, and of different nondimensional thickness $\delta = \ell_D/L$ with ℓ_D the flame thickness and L the burner diameter. The displayed field is nondimensional temperature θ. Flames with $\delta < \delta_c$ where $\delta_c = 0.015$ is the critical value, exhibit DL instability. (a) $\delta = 0.0275 > \delta_c$, (b) $\delta = 0.015 \sim \delta_c$, (c) $\delta = 0.008 < \delta_c$, (d) $\delta = 0.004 < \delta_c$. Note superadiabatic temperatures ($\theta > 1$) issuing from highly curved flame crests. The domain shown is smaller than the entire actual computational domain.

to a weakly turbulent regime, similarly to previous studies such as Ref. [37]. The range of turbulent Reynolds numbers $\mathrm{Re}_t = u_0'\ell/\nu$ spans between 15 and 25, where, for the latter value, the energy spectrum of the streamwise component of the incident flow-field was observed to extend for more than one order of magnitude above and below the integral scale ℓ.

A. Stability limits

Results from the linear stability analysis of a premixed planar flame can be employed to estimate the conditions for which DL instability is promoted in the context of the current deficient reactant flame model to be simulated. Asymptotic dispersion relations were rigorously derived under the deficient reactant assumption [5,38,39]. Such relations, expressing the growth rate $\omega(k)$ of a perturbation of transverse wave number $k = 2\pi/\lambda$, with λ the perturbation wavelength, are usually cast in the form of a series expansion in powers of k, truncated so as to include a linear term expressing the DL hydrodynamic instability and a quadratic stabilizing term due to diffusive effects. In particular Ref. [5] yields a general non-linear hydrodynamic model in which the flame is a gas-dynamic discontinuity between the fresh and burnt mixture, propagating at a flame speed $S_f = S_L^0 - \mathscr{L}\mathbb{K}$, where $\mathbb{K} = S_L^0\kappa + K_S$ is the flame stretch rate inclusive of the effect of curvature κ and hydrodynamic strain K_S and $\mathscr{L}$ is the Markstein length. Given the unit normal $\mathbf{n}$ to the flame, directed towards the burnt gases, then $\kappa = -\nabla\cdot\mathbf{n}$ and $K_s = -\mathbf{n}\cdot\mathbf{E}\cdot\mathbf{n}$, with $\mathbf{E}$ the rate of strain tensor. We note, therefore, that the hydrodynamic model generalizes Markstein's hypothesis, mentioned in the introduction, by including a corrective stretch factor on the flame speed, due to diffusive and reactive processes, ultimately responsible for the short wavelength stabilization. A closed form relation expressing $\mathscr{L}/\ell_D = \mathscr{M}$, where $\mathscr{M}$ is known as the Markstein number, can be rigorously derived from a generalized version of the hydrodynamic model [6] in terms of operative parameters such as σ, Le, and Ze, reading

$$\mathscr{L}/\ell_D = \frac{\sigma}{\sigma-1}\int_1^\sigma \frac{\eta(\tau)}{\tau}d\tau + \frac{\mathrm{Ze}(\mathrm{Le}_{\mathrm{eff}}-1)}{2(\sigma-1)} \times \int_1^\sigma \frac{\eta(\tau)}{\tau}\ln\left(\frac{\sigma-1}{\tau-1}\right)d\tau, \tag{7}$$

where the function $\eta(T/T_u)$ summarizes the temperature dependence of transport coefficients and $\mathrm{Le}_{\mathrm{eff}}$ is an effective Lewis number which is an average of the reactants' Lewis numbers but for off-stoichiometric mixtures coincides with the Lewis number of the deficient reactant. Note that when constant properties are assumed across the flame then $\eta \equiv 1$.

Utilizing a slightly simplified hydrodynamic flame model, in which diffusive effects are retained only in the flame speed expression, it was shown in [40] that a closed form dispersion relation can be derived yielding very similar results to more complete models. In particular by enforcing $\omega = 0$ an expression for the cutoff wavelength is derived, $\lambda_c = 2\pi\mathscr{L}(3\sigma-1)/(\sigma-1)$, so that the flame is hydrodynamically unstable to any perturbation of wavelength λ such that $\lambda_c < \lambda < L$. Equivalently, the instability condition $\lambda_c < L$, dividing by ℓ_D, translates into $\delta < \delta_c$ where $\delta_c = \ell_D/\lambda_c$. Thus planar flames exhibiting nondimensional thickness smaller than the critical value δ_c are hydrodynamically unstable. This concept holds unaltered for slot flames for which the diameter L represents the minimum hydrodynamic length. Note, therefore, that DL instabilities can be induced by decreasing the thickness of the flame relative to the hydrodynamic length L. This can be accomplished by increasing the operative pressure, driving the composition towards stoichiometry or simply by increasing L.

In order to estimate δ_c, Eq. (7) is used to estimate $\mathscr{L}/\ell_D$ as a function of the operative parameters, where $\eta \equiv 1$ is assumed to enforce constant properties, similarly to the deficient reactant model Eqs. (1)–(3). To illustrate the stability limits we derive the maximum number of unstable wavelengths

$$n_c = L/\lambda_c = (\sigma-1)/\{2\pi(\mathscr{L}/\ell_D)\delta(3\sigma-1)\}, \tag{8}$$

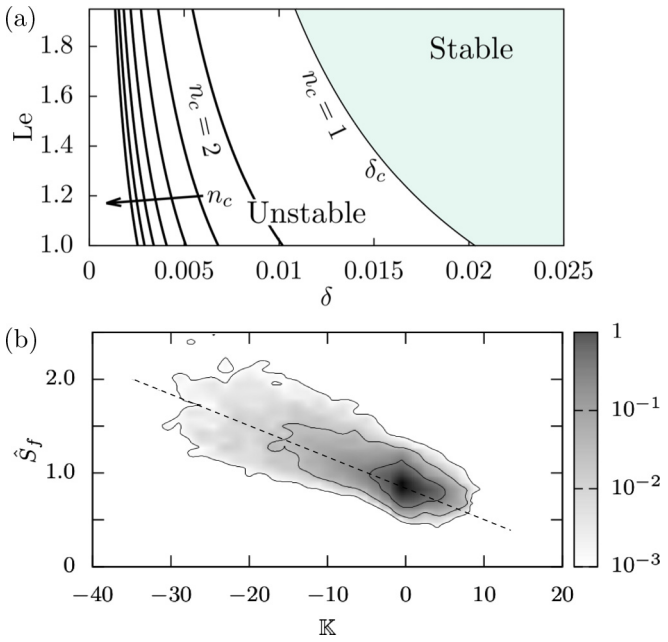

FIG. 4. (a) Number of unstable wavelengths n_c as a function of δ and Le. Stability region corresponds to $n_c \leqslant 1$. (b) Direct estimation of $\mathscr{L}/\ell_D$ from the slope of the linear regression model (dashed line) between (nondimensional) local normalized flame speed and stretch rate. Color map shows the normalized joint p.d.f. of flame speed and stretch obtained from a simulated flame at $\delta = 0.008$ and using $\theta^* = 0.8$.

which is displayed in Fig. 4(a) as a function of δ and Le all other parameters being constant. The locus $n_c = 1$ is clearly the stability boundary and thus represents the function $\delta_c(\mathrm{Le},\sigma,\mathrm{Ze})$. Using the parameters of Table I we obtain $\mathscr{L}/\ell_D \approx 2.8$ corresponding to $\delta_c \approx 0.017$.

Alternatively, $\mathscr{L}/\ell_D$ can be estimated directly from the simulations. Given the asymptotic linear relation between flame speed and stretch, the Markstein number can be recovered from the slope of a linear regression model between computed local values of said variables. The local stretch rate $\mathbb{K}$ is computed by choosing an iso-surface representative of the flame, such as $\theta(x,y,t) = \theta^*$, and determining the local curvature and hydrodynamic strain. The local instantaneous flame speed S_f, on the other hand, is assumed as the local displacement speed [41,42], defined as the flame speed relative to the local normal flow velocity, and is derived by following the motion of the iso-surface $\theta = \theta^*$, whose dynamics is described by a level-set equation of the kind

$$S_f \left(\frac{\partial\theta}{\partial x_i}\frac{\partial\theta}{\partial x_i} \right)^{1/2} \Bigg|_{\theta=\theta^*} = \left(\frac{\partial\theta}{\partial t} + u_j \frac{\partial\theta}{\partial x_j} \right) \Bigg|_{\theta=\theta^*}, \qquad (9)$$

where the material derivative is computed from the right hand side of Eq. (3). The displacement speed in Eq. (9) is clearly sensitive to the choice of θ^* given that such choice determines the local value of density ρ^* and thus of mass flow and incident velocity. To eliminate the dependence from θ^*, the displacement speed is normalized by the local density ratio [41], thus yielding $\hat{S}_f = S_f \rho^*/\rho_u$. Figure 4(b) displays the joint probability density function (p.d.f.) between the normalized displacement speed and stretch, highlighting the linear regression model (dashed line), the slope of which yields an estimate of the Markstein number $\mathscr{L}/\ell_D \approx 2.8$, sufficiently close to the value obtained using Eq. (7), corresponding to $\delta_c \approx 0.02$. The value of θ^* used in Fig. 4(b) was chosen to represent an iso-surface close to the burned side, consistently with the findings in Ref. [41]. The values of δ selected for the simulations, shown on Table I, were, in conclusion, clearly chosen so as to encompass the bifurcation value δ_c.

B. Results: Morphology and propagation of turbulent flames

As mentioned in the Introduction, we now address the first issue of unambiguously establishing the presence or absence of DL-induced morphological features on turbulent premixed flames. It is widely recognized from experimental [9], numerical [12,40,43], and analytical studies [44,45] that DL instability induces a characteristic cusp-like wrinkling on a freely propagating planar laminar flame which acts as a morphological signature for DL effects. During the linear growth phase, a flame perturbation will exponentially grow in amplitude until, in the non linear phase, the DL growth is contrasted by the Huygens principle of normal propagation and the flame is stabilized into a finite amplitude, cusp-like conformation [46]. In a fully laminar setting, such cusp-like cells will coalesce into a unique steady cell, encompassing the entire hydrodynamic domain [26]. Given the associated flame area increase with respect to the planar conformation, the steady propagation speed U of a flame exhibiting DL instability will be substantially higher than the reference, unstretched, laminar speed of a stable planar flame S_L^0. A measure of such increase can be obtained from the Sivashinsky equation [47] and its modifications [48] for which the flame speed can be derived analytically. For example, in Ref. [48] an expression is derived for the nondimensional steady propagation speed in the form $U/S_L^0 = 1 + U_m(\sigma) f(\delta/\delta_c)$. Figure 5 displays such propagation speed as a function of δ/δ_c and clearly exhibits the bifurcative behavior for $\delta/\delta_c < 1$ accompanied by a substantial increase in speed.

Shifting our attention to turbulent flames, previous studies [23,26] have shown that the characteristic, DL-induced, cusp-like morphology persists, exhibiting highly curved crests and smoother, wider troughs which introduce an asymmetric distribution of flame surface curvature. In other words, when the planar flame loses stability, in addition to turbulence-driven

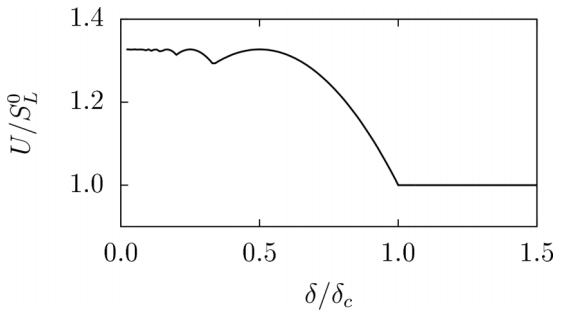

FIG. 5. Steady laminar propagation speed, scaled with the planar speed S_L^0, for a planar flame experiencing DL instability. The model is derived from the Sivashinsky equation and corrected [48] for finite expansion ratio σ (case shown $\sigma = 8$).

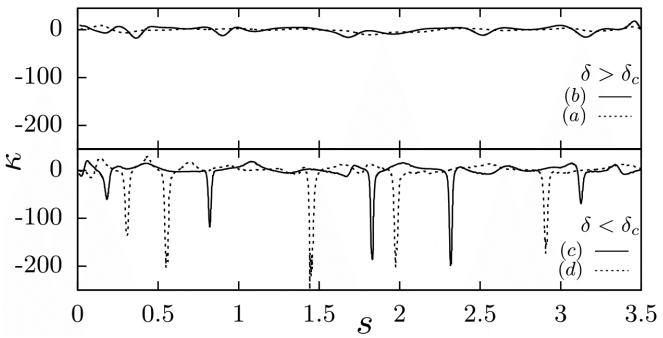

FIG. 6. Curvature of iso-contour $\theta = \theta^*$ along the flame coordinate s. Upper and lower panel display curvature profiles, respectively, for the stable and unstable flames displayed in Fig. 3.

wrinkling it exhibits localized bursts of negative curvature (provided the flame normal is in the direction of burnt gases) corresponding to crests and more moderate positive curvatures corresponding to troughs. On the other hand, a flame for which the planar conformation is stable will not exhibit any bias on curvature once wrinkled by turbulence. Figure 6 displays the flame curvature for a stable ($\delta > \delta_c$) and an unstable ($\delta < \delta_c$) slot flame selected from the present turbulent simulations, shown in Fig. 3. Thus, even in a mildly turbulent setting, we observe a dramatic morphological dichotomy between stable and unstable flames, similarly to the bifurcative behavior shown for laminar flames in Fig. 5, which suggests that the statistical properties of curvature can act as an unambiguous marker for DL effects. In particular, the skewness of curvature p.d.f., measuring its asymmetry about the mean, is an observable expected to act as such marker. We note that some authors [49] have observed other features such as transient unburned mixture fingers which can also induce a preferentially negative flame curvature, although this phenomenon was not linked to DL-instability and is therefore not expected to increase or decrease its intensity as δ is varied across the bifurcation value δ_c.

Figure 7 displays curvature p.d.f.'s for selected simulated flames which clearly exhibit a pronounced skewness towards negative curvatures for δ below the bifurcation value δ_c while, above such value, distributions are largely more symmetrical

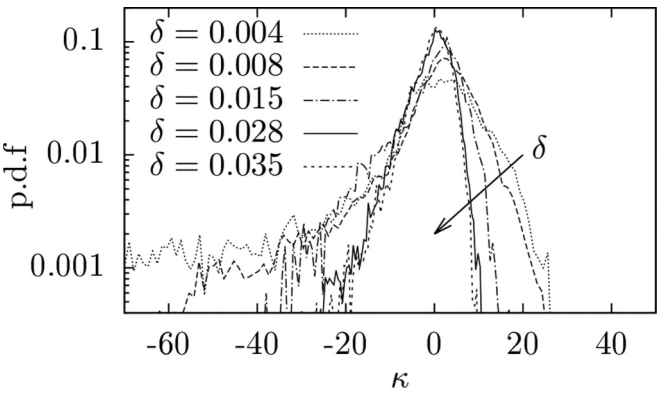

FIG. 7. Probability density function of curvature for stable ($\delta_c = 0.017 < \delta = 0.028, 0.035$) and unstable ($\delta_c > \delta = 0.015, 0.004, 0.008$) flames.

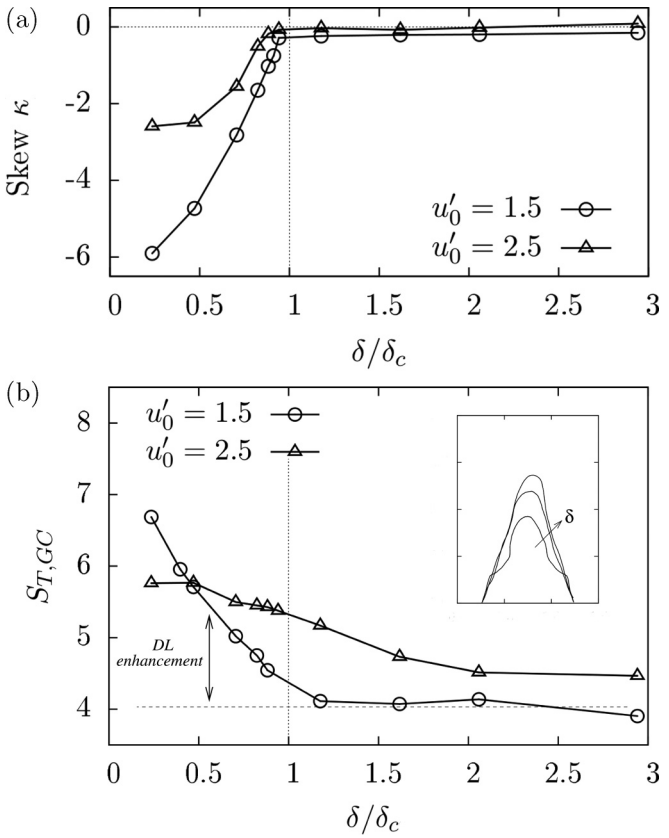

FIG. 8. (a) Skewness of flame curvature distribution versus δ/δ_c for two values of turbulence intensity. (b) Turbulent burning velocity versus δ/δ_c for two values of turbulence intensity. Inset: Time-averaged concentration iso-contours $Y = Y^* = 0.9$ for $\delta = 0.008, 0.015, 0.00675$, and $u_0' = 1.5$.

and insensitive to variations of δ. Indeed Fig. 8(a) clearly and unambiguously shows that a nondimensional parameter such as the skewness of the curvature distributions, characterizing their degree of symmetry, exhibits a threshold behavior whereby for $\delta > \delta_c$ it is insensitive to variations of the parameter δ, highlighting a wrinkled flame surface devoid of a preferential curvature, while for $\delta < \delta_c$ the skewness experiences a dramatic drop, becoming highly sensitive to δ, a manifestation of the presence of localized, preferentially curved structures of increasingly negative curvature. We also note that a lower moment such as the mean or variance of the curvature, while still exhibiting a different behavior for stable and unstable flames, is less effective as a marker as it lacks the clear threshold behavior of skewness. In addition, while lower moments such as mean or variance are not invariant under a linear transformation of the random variable, skewness is indeed invariant and as such it is independent of any renormalization of curvature, e.g., such as the rescaling of curvature by the thickness δ.

A first conclusion that can be drawn from the simulations is that an observable such as the skewness of curvature distribution will likely act as an unambiguous marker for DL instability effects also in the context of experimental slot or Bunsen flames. In an experimental setting, control of the bifurcation parameter $\delta = \ell_D/L$ will be achieved either by varying the slot or Bunsen diameter L and/or by varying the

flame thickness ℓ_D through stoichiometry and/or pressure. In the following sections we verify this through an experimental analysis of propane or air turbulent Bunsen flames.

We now focus our attention on the turbulent burning velocity of the slot flames and, in particular, how this is affected by the onset of DL instability and by the intensity of the incident turbulence. The concept of global consumption speed $S_{T,GC}$ [50] as a definition for turbulent burning velocity S_T is particularly suited to slot or Bunsen geometries. Because all of the supplied fresh mixture passes through the flame, mass conservation implies that the inlet mass flow rate be expressed as $\dot{m} = \rho_u S_{T,GC} A_{\overline{Y}=Y^*}$ where $S_{T,GC}$ is the effective burning velocity of the turbulent flame of area $A_{\overline{Y}=Y^*}$ corresponding to the time-averaged generic iso-contour $Y = Y^*$. The inset in Fig. 8(b) displays time-averaged iso-contours for representative values of δ at a fixed turbulence intensity. While such time-averaged iso-contours exhibit some degree of residual asymmetry, their area was found to have reached sufficient statistical convergence which is of relevance in the determination of the turbulent burning velocity. It is apparent that as δ is decreased below the critical value, the effect of the DL-induced flame morphology is to decrease the area $A_{\overline{Y}=Y^*}$ of such averaged iso-contour. Given the constant mass flow, such a decrease is accompanied by a corresponding increase in the turbulent burning velocity which is, in turn, caused by an increase in the instantaneous area per unit flame length or flame surface density (a measure of the average flame surface to volume ratio). This effect is evident in Fig. 3 where as δ is decreased the flame wrinkling and thus the instantaneous flame area per unit flame length is observed to increase and, concurrently, the flame height is observed to decrease due to mass continuity.

Indeed Fig. 8(b) clearly shows that for the same (low) turbulence intensity $u'_0 = 1.5$, Lewis number and expansion ratio, two clearly distinct turbulent propagation regimes exist, characterized by the absence or presence of DL instability. In particular, for $\delta > \delta_c$ a regime exists for which the turbulent burning velocity is insensitive to variations of δ while for $\delta < \delta_c$ a different regime ensues where S_T becomes highly sensitive to δ and a DL-driven enhancement of S_T is observed. The consequence of this on laboratory flames is the following: given a combustible mixture, of fixed composition and at a given pressure, thus yielding a given flame thickness ℓ_D, two distinct turbulent propagation regimes exist for the same turbulence intensity u'_0. Such regimes can be triggered by varying the hydrodynamic length L (e.g., the diameter of a Bunsen burner) so as to promote ($\delta < \delta_c$) or suppress ($\delta > \delta_c$) DL instabilities.

The above arguments address the second question which was put forth in the introduction regarding the effect of DL instability on the flame morphology and turbulent propagation. In the following sections we will verify the foregoing observations in the context of an experimental Bunsen flame. The third question, on the other hand, addressed the impact of turbulence intensity in mitigating or even suppressing the role of DL instability in the turbulent flame morphology and propagation. Increasing the turbulence intensity to $u'_0 = 2.5$, Fig. 8(a) shows a pronounced decrease in the sensitivity of curvature skewness to δ, for $\delta < \delta_c$, while the discussed threshold behavior seems to persist, albeit in a less noticeable form. This essentially suggests that the turbulence generated wrinkling has a mitigating function on the DL-induced flame morphology. Similarly, at such higher turbulence intensity, Fig. 8(b) exhibits a far reduced sensitivity of the turbulent burning velocity to δ while the dual behavior caused by DL effects and observed at lower intensity seems to disappear completely. This also suggests that the increase in flame area per unit flame length induced by DL effects alone, is mitigated by the effect of turbulence generated wrinkling. Also noteworthy is that, contrary to the lower intensity case or even to the representative laminar scenario depicted in Fig. 5, at higher intensity the effect of DL instability extends to an entire range of values of δ protruding away from the bifurcation point into the stable region. This behavior was also observed in a number of previous studies utilizing a variety of methods such as the stochastic Sivashinsky equation [13] or a hybrid level set methodology [27,37]. While still unproven, it is to be expected that a further increase in intensity would completely overshadow any effect due to hydrodynamic instability, thus eliminating any residual functional dependence of curvature skewness or S_T on the parameter δ. To conclude, these findings suggest that DL effects on the turbulent propagation of a premixed flame are clearly evident and noticeable albeit strictly confined to a low turbulence intensity regime.

III. EXPERIMENTAL INVESTIGATION

The effects of DL instability on an experimental propane (C_3H_8) or air Bunsen flame at atmospheric pressure are now investigated. Similar guidelines to those followed in the numerical investigation are used. In particular, results from asymptotic theory are utilized in order to estimate the critical flame thickness δ_c as a function of the equivalence ratio ϕ which, in the experimental campaign, acts as an independent parameter. The nondimensional flame thickness $\delta = \ell_D/L$ is varied either by varying ϕ, which acts on ℓ_D, or by adopting a different Bunsen diameter L. Because DL instability is triggered for $\delta < \delta_c$, two Bunsen diameters are chosen in such a way that unstable conditions are always met for the larger diameter while stable conditions, $\delta > \delta_c$, are consistently met for the smaller diameter, irrespective of the equivalence ratio ϕ used.

To estimate δ_c we need to adapt any asymptotic model and ensuing dispersion relation to the propane or air mixture used in experiments. In particular, by fitting experimental data by Tseng *et al.* [51] for propane or air mixtures at atmospheric pressure, we derive the functional dependence of all the relevant operative parameters from the equivalence ratio, namely $\sigma(\phi)$, $S_L^0(\phi)$, and $T_{ad}(\phi)$. In Sec. II A, a slightly simplified hydrodynamic model was utilized yielding a dispersion relation for the deficient reactant model, derived by Creta and Matalon in Ref. [40], which we refer to here as the CM dispersion relation. This can be adapted to propane or air mixtures by using in Eq. (7) a temperature dependent transport coefficient, i.e., $\eta(T/T_u) = (T/T_u)^\gamma$ and an effective Lewis number representing a weighed average of the fuel and oxidizer Lewis numbers as described in [6,52]. The exponent γ is usually taken as a constant between $1/2$ and 1.

The most general dispersion relation, however, was derived by Matalon, Cui, and Bechtold [6] directly for a two reactant mixture, and is referred to here as MCB. In its dimensional

form the MCB dispersion relation reads [6]

$$\omega(k) = \omega_0\, S_L^0\, k - \mathcal{D}_{th}\, \omega_1\, k^2, \qquad \omega_1 = B_1 + \mathrm{Ze}(\mathrm{Le_{eff}} - 1)B_2 + \mathrm{Pr}B_3, \tag{10}$$

where $\omega_0 = (-\sigma + \sqrt{\sigma^3 + \sigma^2 - \sigma})/(\sigma + 1)$, Pr is the Prandtl number and B_1, B_2, and B_3 are coefficients, functions of σ, whose expression can be found in Ref. [6]. It is easily verified that for the MCB relation the critical thickness reads $\delta_c = \omega_0/(2\pi\omega_1)$.

Additional models were used, such as the one formulated by Pelce and Clavin [38], which we refer to as PC, who derive a dispersion relation in the form

$$\omega(k) = \Omega\, S_L^0\, k \qquad \Omega = \frac{\sigma}{\sigma - 1}\{[\omega_3 + \mathscr{L}k(\mathscr{L}k - 2\sigma)]^{1/2} - \mathscr{L}k - 1\}, \tag{11}$$

where $\omega_3 = (\sigma^2 + \sigma - 1)/\sigma$ and where the effect of gravity was neglected. An expression for the Markstein number was derived by Clavin and Garcia [53] which accounts for temperature dependent diffusivities. In particular, using the dependence given by the kinetic theory of gases in the approximation of rigid sphere, corresponding to an exponent $\gamma = 1/2$, such expression is given by

$$\mathscr{L}/\ell_D = \frac{2\sigma}{\sqrt{\sigma + 1}} + \mathrm{Ze}(\mathrm{Le_{eff}} - 1)\left[\frac{2}{\sqrt{\sigma + 1}} - \frac{\sigma}{\sigma - 1}\ln\left(\frac{\sqrt{\sigma} + 1}{2}\right)\right]. \tag{12}$$

Finally the PC model was used similarly to Ref. [25] using Eq. (7) for the Markstein length to generalize the temperature dependence. We refer to the latter model as PC1.

Figure 9 displays the critical flame thickness δ_c as a function of the equivalence ratio ϕ as estimated by the foregoing models. Regardless of the temperature exponent used, provided it is chosen in the range $\gamma \in [1/2, 1]$, all models seem to yield similar results, with only a slight variability with ϕ, around the average value $\delta_c \approx 0.006$. As mentioned, this value acts as a guideline for the choice of the Bunsen diameters. In other words, given the flame thickness dependence on equivalence ratio for propane or air mixtures at atmospheric pressure, $\ell_D(\phi)$, the Bunsen diameter L is chosen so that in order to trigger DL instabilities $\delta(\phi) = \ell_D(\phi)/L < \delta_c \approx 0.006$ in the range of ϕ of interest, and otherwise if instabilities are to be suppressed. This analysis yields a 'large' diameter, chosen as $L = 18$ mm, for which $\delta(\phi) < \delta_c$, at least in a wide range of near-stoichiometric mixtures which, observing Fig. 9, can be roughly estimated as $\phi \in [0.7, 1.6]$. Thus, such diameter is expected to be larger than the cutoff wavelength and therefore to exhibit DL instabilities. A 'small' diameter $L = 9$ mm is also identified, for which $\delta(\phi) > \delta_c$ for all values of ϕ, which is systematically smaller than the estimated cutoff wavelength at each ϕ and thus expected to be unable to sustain instabilities. In a previous experimental study [23] the presence of DL instability was conjectured based on similar considerations and on flame curvature albeit using a single Bunsen diameter. The use of the additional smaller diameter, which is expected to suppress instabilities, is intended here to serve the purpose of unambiguously highlighting morphological differences between stable and unstable flames.

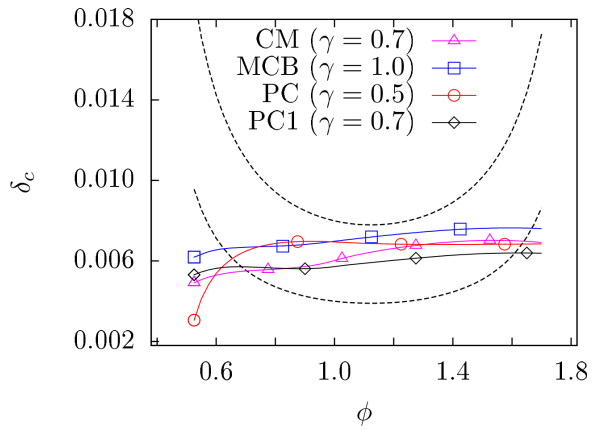

FIG. 9. Critical nondimensional flame thickness δ_c as a function of equivalence ratio ϕ for propane or air mixtures, using different dispersion relation models (notation defined in the text) and different exponents γ for temperature dependence of transport coefficients. Dashed curves represent the nondimensional flame thickness $\delta = \ell_D/L$ for two Bunsen diameters: $L = 18$ mm (lower dashed curve) and $L = 9$ mm (upper dashed curve). All pertinent data for propane or air mixtures was taken from Ref. [51] while diffusivities were taken from Ref. [52].

A. Experimental results

The experimental setup is similar to that described in [23,54,55]. As mentioned, two Bunsen diameters are utilized and the ensuing flames analyzed by means of a PIV setup using a laser source of 54 mJ Nd:YAG equipped with a 60 mm focal length camera working at a resolution of 1024 × 1280 pixels. The range of composition and bulk Reynolds numbers tested is reported in Table II, where $\mathrm{Re} = 4\dot{m}/(\mu\pi L)$ with $\dot{m}$ the reactive mixture flow rate and μ the dynamic viscosity. Note that the latter definition differs from that given in Sec. II. The flame front position is determined from the sudden jump in alumina particle number density caused by the flame zone expansion which, in Mie scattering images, corresponds to zones at very different levels of scattered light intensity. Thus an intensity threshold easily identifies the flame surface. Image postprocessing yields global quantities such as flame surface area (under the hypothesis of axis-symmetric flame) and local quantities such as flame curvature. Thus, turbulent burning velocities, defined as the global consumption speed introduced previously, are easily recovered from the average flame front position while morphological properties can be extracted from the p.d.f.'s of curvature [23].

Additional parameters of interest for the experimental campaign, characterizing the incident flow field, are given in

TABLE II. Main parameters used in the experimental investigation of C_3H_8/Air flames at atmospheric pressure.

L [mm]	ϕ	Re
9.0,18.0	0.7–1.8	2500–7000

TABLE III. Main experimental flow parameters corresponding to unreactive cases ($\phi = 0$). Velocities are expressed in ms^{-1} while the correlation length ℓ in mm.

$L = 9$ mm					$L = 18$ mm				
Re	Re_t	U_{CL}	u'_0	ℓ	Re	Re_t	U_{CL}	u'_0	ℓ
2500	–	5.2	0.1	–	2500	–	3.2	0.19	–
5000	20	9.8	0.5	0.6	5000	38	5.9	0.6	0.96
7000	29	13.4	1.1	0.4	7000	43	6.8	1.0	0.65

Table III for representative unreactive cases, corresponding to equivalence ratio $\phi = 0$. In particular, the mean of the axial velocity U_{CL} and its root mean square u'_0, calculated at the centerline, away from the wall boundary layer influence, are reported, both expressed in ms^{-1}. The last column reports the correlation length ℓ (expressed in mm) defined as the integral of the autocorrelation coefficient of the axial velocity. For each bulk Reynolds number, the turbulent Reynolds number $Re_t = u'_0\ell/\nu$ is also given. All the quantities have been evaluated at 5 mm above the jet nozzle exit (see Ref. [56] for details). For case at Re $= 2500$ (considered laminar) the correlation coefficient is not reported.

Figure 10 shows the different morphological features of two sets of flames obtained with the two different Bunsen diameters $L = 18$ and 9 mm at the same Reynolds number and for the same range of equivalence ratios. In particular,

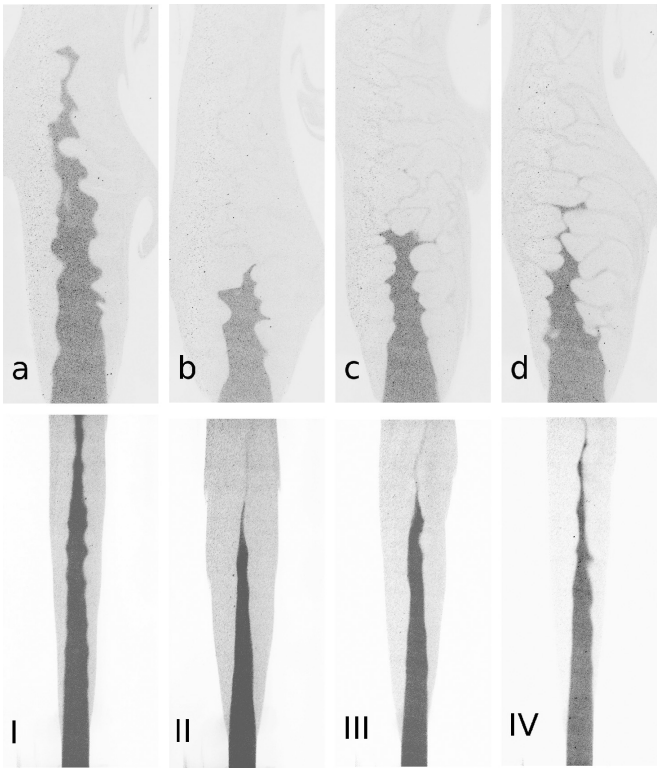

FIG. 10. Mie scattering images of C_3H_8/Air flames at Re $=$ 5000. Upper panels: Bunsen diameter $L = 18$ mm. Lower panels: $L = 9$ mm. Flames a-d and I-IV correspond to $\phi = 0.8, 1.1, 1.4, 1.5$, respectively.

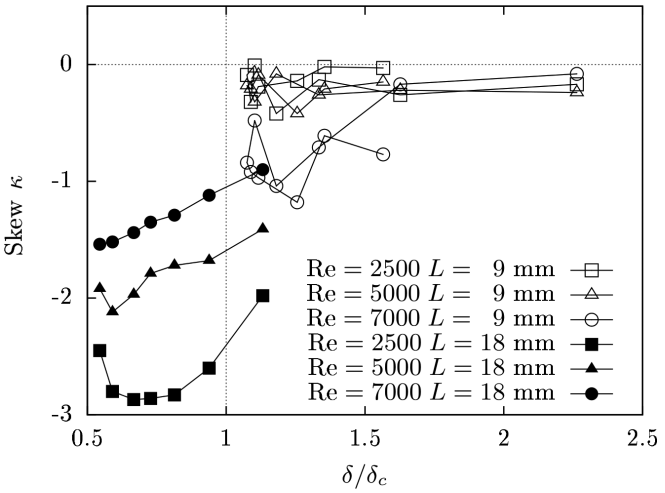

FIG. 11. Skewness of flame curvature versus δ/δ_c for experimental C_3H_8/Air flames at Re $= 2500$–7000 using two Bunsen diameters $L = 9$ and 18 mm. Range of equivalence ratio for smaller diameter is $\phi \in [0.8, 1.7]$ while for larger diameter $\phi \in [1.1, 1.7]$.

signature effects due to DL instability are visible for the larger diameter in terms of cusp-like wrinkling, while these effects are absent for the smaller diameter. Following the conclusions of the numerical campaign, we now monitor the instability marker, identified as the skewness of the flame curvature p.d.f.. This is shown in Fig. 11 as a function of δ/δ_c where δ_c is estimated with the CM model of Fig. 9 (albeit no significant difference is noticed using other models). Similarly to numerical simulations results of Fig. 8(a), we observe a clearly distinct behavior of curvature skewness depending on whether $\delta/\delta_c > 1$ or < 1. Skewness levels are related to the largest absolute curvature that can be evaluated, which, for experiments, is limited to the image resolution of $\sim$90 μm and to flame thickness which varies in the range 50–100 μm. Note that for each Bunsen diameter, data points on the iso-Re curves are obtained by varying the equivalence ratio ϕ. In particular, for the smaller diameter, data is confined to $\delta/\delta_c > 1$ and curvature skewness, which is only mildly negative, seems to be insensitive to variations of equivalence ratio. This behavior is coherent with the absence of DL instabilities, as shown by the numerical analysis. On the other hand, for the larger diameter, data is almost entirely confined to $\delta/\delta_c < 1$ and the skewness becomes abruptly negative and highly sensitive to variations of equivalence ratio, a behavior coherent with the presence of DL-induced morphology. This confirms, in an experimental setting, the dichotomic behavior of flame morphology with respect to variations of the parameter δ. Note that, as expected, the abrupt change in skewness is most evident at the lowest bulk Reynolds number, which is considered laminar, thus excluding a possible additional role, other than that played by δ, of the turbulent scale ℓ in the onset of such behavior. Turbulence intensity, on the other hand, will play a role in mitigating such effect, as explained below.

Observing Fig. 11 and following the data sets for increasing Re numbers, we also observe a decrease in the abrupt drop in curvature skewness as $\delta/\delta_c < 1$ for higher Reynolds. In this context, the bulk Re can be directly related to turbulence

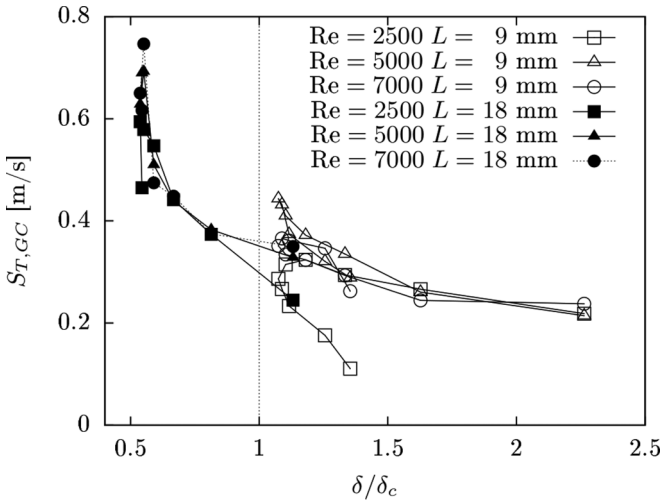

FIG. 12. Turbulent burning velocity versus δ/δ_c for experimental C_3H_8/Air flames at Re = 2500–7000 using two Bunsen diameters $L = 9$ and 18 mm.

intensity (see Table III), thus indicating a similar behavior to Fig. 8(a) whereby higher intensity translates to a reduced sensitivity of skewness to δ. This is particularly evident for the Re = 7000 data set of Fig. 11, corresponding to the highest turbulent intensity examined, for which skewness does not seem to exhibit a sudden drop as δ/δ_c is decreased below unity, but rather it seems to be subject to a uniform decrease.

Finally, for the same experimental data sets, in Fig. 12 we monitor the dimensional turbulent burning velocity S_T, evaluated as the global consumption speed $S_{T,GC}$. Similarly to the numerical findings [Fig. 8(b)], we observe two different regimes of turbulent propagation. While for $\delta > \delta_c$ the turbulent propagation speed seems to be less sensitive to variations of δ, for $\delta < \delta_c$, corresponding to the larger Bunsen diameter, a DL-driven regime ensues for which the turbulent propagation speed is enhanced and becomes highly sensitive to δ. Indeed, Fig. 12 suggests that the presence of DL-induced flame corrugation can more than double the turbulent propagation speed at a given Reynolds number and mixture composition.

Contrary to numerical simulations where δ is an independent parameter, in experiments the ratio δ/δ_c is varied by using two different Bunsen diameters and by varying the equivalence ratio, which implies a variation in laminar flame speed. Figure 13 displays the turbulent flame speed adequately rescaled with respect to the unstretched laminar flame speed S_L^0. While the data in Fig. 13 reflect the fact that for each of the two Bunsen diameters, smaller values of δ correspond to higher values of S_L^0, it still exhibits a clear amplification of the normalized turbulent speed when $\delta < \delta_c$, similarly to Fig. 12. Figure 14 shows the enhancement of turbulent propagation speed between the Bunsen diameter $L = 18$ mm flames and $L = 9$ mm flames at each corresponding equivalence ratio, which reaches a factor of two at $\phi = 1.2 \sim 1.3$ with a tendency to decrease as ϕ increases. Note from Fig. 13 that for some lean flames ($\phi = 0.8, 0.9, 1.0$) at the lowest Reynolds number of 2500, we observe $S_{T,GC}/S_L^0 < 1$. A tentative explanation for this may be found in the effect of buoyancy, which may

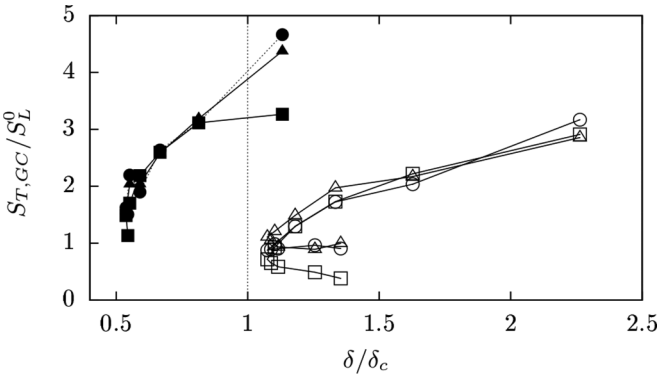

FIG. 13. Turbulent burning velocity normalized with laminar flame speed versus δ/δ_c. Notation is identical to Figs. 11 and 12.

play a role at the lowest Re and which was found in Ref. [57] to induce longer turbulent Bunsen flames in lean conditions, corresponding to lower values of $S_{T,GC}$.

As we have seen, the numerical campaign suggests that an increase of turbulence intensity causes a decrease of both flame curvature skewness and turbulent propagation speed sensitivity to variations of δ as it is decreased below the critical value δ_c. While this seems to be confirmed in experiments for the curvature skewness (Fig. 11), the variation of the Reynolds number does not cause appreciable changes in the sensitivity of S_T on δ. Higher Reynolds numbers should possibly be investigated in order to observe such an effect.

IV. SUMMARY

In this investigation we performed two-dimensional numerical simulations of slot burner premixed turbulent flames as well as experiments of C_3H_8/Air turbulent Bunsen flames with the objective of (i) unambiguously identifying the effect of Darrieus-Landau (DL) instability on the morphology and propagation of turbulent premixed flames, (ii) quantifying such an effect and, finally (iii) assessing whether the increase of turbulence intensity mitigates or even suppresses such effect.

The numerical campaign is based on a deficient reactant model which enables the coherent use of results obtained within linear stability analysis, thus allowing the unambiguous

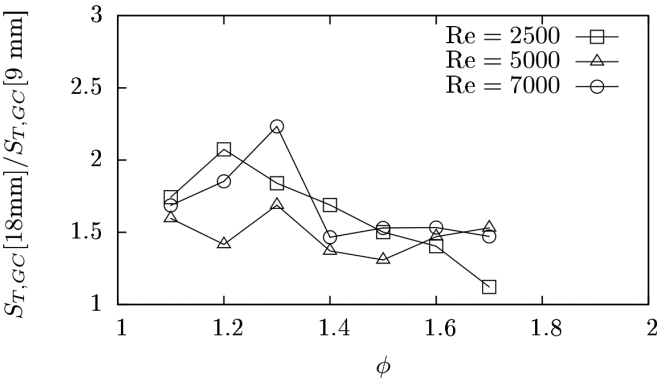

FIG. 14. Enhancement (ratio) of turbulent burning velocity between Bunsen diameter $L = 18$ mm flames and $L = 9$ mm flames.

identification of the stability limits in terms of an independent parameter δ, measuring the flame thickness nondimensionalized with respect to the slot width. As $\delta < \delta_c$, where δ_c is the bifurcation value, DL instability dramatically changes the morphological features of the turbulent flame. We identify the skewness of the flame curvature p.d.f. as an unambiguous marker for the presence of DL-induced effects. In particular, in the absence of DL instability, skewness remains insensitive to variations of δ, while for $\delta < \delta_c$ a bifurcative effect is observed with the skewness becoming highly sensitive to δ. As a results of such dichotomic behavior of flame morphology with respect to variations of the parameter δ, we observe a similar dual behavior in the turbulent propagation of the flame. In particular, for the same turbulence intensity and expansion ratio, the onset of DL instability is observed to cause a sudden increase in the turbulent propagation speed which is otherwise insensitive to variations of δ. An increase in turbulence intensity tends to attenuate such sharp, dual behavior, mitigating the effect of DL instability, thus suggesting it is a feature limited to low turbulence intensity regimes of propagation.

Experimental C_3H_8/Air turbulent Bunsen flames are also analyzed via a PIV setup. The bifurcation parameter δ_c is estimated by adapting several analytical asymptotic models to propane or air mixtures. DL instability is then triggered by adopting two Bunsen diameters and concurrently varying the equivalence ratio. Experimental flames, similarly to numerical simulations, exhibit a clear dichotomic behavior of flame morphology, with the curvature skewness becoming extremely sensitive to variations of δ when $\delta < \delta_c$ while remaining insensitive to δ for $\delta > \delta_c$. A similar dual behavior and enhanced sensitivity is also observed in terms of the turbulent propagation speed. In addition, Reynolds number effects, connected to turbulence intensity effects, are also analyzed. While the sensitivity to δ of curvature skewness is observed to decrease with Re, no appreciable effect is observed for the turbulent propagation speed, possibly suggesting that higher Re numbers should be investigated in order for turbulence to have a mitigating effect over DL-induced effects.

ACKNOWLEDGMENTS

Participants of this study were financially supported by the Italian Ministry of University and Research Ministero dell'Istruzione, Universitá e della Ricerca (MIUR). The authors acknowledge the Italian Super-Computing Interuniversity Consortium CINECA for support and high-performance computing resources under Grant No. DL-3D/HP10CRXOHF.

[1] G. Darrieus, Propagation d'un front de flamme, unpublished work, presented at La Technique Moderne (Paris) and in 1945 at Congrès de Mécanique Appliquée.
[2] L. Landau, Zh. Eksp. Teor. Fiz. **14**, 240 (1944); Acta Phys.-Chem. USSR **19**, 77 (1944).
[3] G. Markstein, *Nonsteady Flame Propagation* (Macmillan, New York, 1964).
[4] P. Clavin and F. A. Williams, J. Fluid Mech. **90**, 589 (1979).
[5] M. Matalon and B. Matkowsky, J. Fluid Mech. **124**, 239 (1982).
[6] M. Matalon, C. Cui, and J. Bechtold, J. Fluid Mech. **487**, 179 (2003).
[7] H. Guenoche and M. Jouy, Proc. Combust. Inst. **4**, 403 (1952).
[8] R. Petersen and H. Emmons, Phys. Fluids **4**, 456 (1961).
[9] C. Clanet and G. Searby, Phys. Rev. Lett. **80**, 3867 (1998).
[10] Y. A. Gostintsev, A. G. Istratov, and Y. V. Shulenin, Combustion, Explosions and Shock Waves **24**, 563 (1988).
[11] F. Wu, G. Jomaas, and C. K. Law, Proc. Combust. Inst. **34**, 937 (2013).
[12] S. I. Blinnikov and P. V. Sasorov, Phys. Rev. E **53**, 4827 (1996).
[13] F. Creta, N. Fogla, and M. Matalon, Comb. Th. and Modelling **15**, 267 (2011).
[14] R. Yu, X. S. Bai, and V. Bychkov, Phys. Rev. E **92**, 063028 (2015).
[15] V. R. Kuznetsov, Combustion, Explosions, and Shock Waves **18**, 172 (1982).
[16] P. Cambray and G. Joulin, Proc. Combust. Inst. **24**, 61 (1992).
[17] A. Klimenko, Combust. Sci. Technol. **139**, 15 (1998).
[18] V. Bychkov, Phys. Rev. E **68**, 066304 (2003).
[19] V. Akkerman and V. Bychkov, Comb. Th. and Modelling **9**, 323 (2005).
[20] H. Kobayashi and H. Kawazoe, Proc. Comb. Inst. **28**, 375 (2000).
[21] V. Savarianandam and C. Lawn, Combust. Flame **146**, 1 (2006).
[22] D. Bradley, M. Lawes, L. Kexin, and M. Mansour, Proc. Comb. Inst. **34**, 1519 (2013).
[23] G. Troiani, F. Creta, and M. Matalon, Proc. Comb. Inst. **35**, 1451 (2015).
[24] A. Lipatnikov and J. Chomiak, Prog. Energy Combust. Sci. **31**, 1 (2005).
[25] S. Chaudhuri, V. Akkerman, and C. K. Law, Phys. Rev. E **84**, 026322 (2011).
[26] F. Creta and M. Matalon, J. Fluid Mech. **680**, 225 (2011).
[27] N. Fogla, F. Creta, and M. Matalon, Combust. Flame **162**, 2758 (2015).
[28] A. Patera, J. Comput. Phys. **54**, 468 (1984).
[29] M. O. Deville, P. F. Fischer, and E. H. Mund, *High-Order Methods for Incompressible Fluid Flow, Part of Cambridge Monographs on Applied and Computational Mathematics* (Cambridge University Press, 2002).
[30] J. W. L. Paul F. Fischer, and S. G. Kerkemeier, nek5000 web page (2008), http://nek5000.mcs.anl.gov.
[31] A. Tomboulides, J. Lee, and S. Orszag, J. Sci. Comp. **12**, 139 (1997).
[32] A. C. Hindmarsh, P. N. Brown, K. E. Grant, S. L. Lee, R. Serban, D. E. Shumaker, and C. S. Woodward, ACM Transactions on Mathematical Software (TOMS) **31**, 363 (2005).
[33] S. G. Kerkemeier, Direct numerical simulation of combustion on petascale platforms, Ph.D. thesis, Diss., Eidgenössische Technische Hochschule ETH Zürich, No. 19162, 2010 (2010).
[34] S. Kerkemeier, C. Markides, C. Frouzakis, and K. Boulouchos, J. Fluid Mech. **720**, 424 (2013).
[35] M. Klein, A. Sadiki, and J. Janicka, J. Comput. Phys. **186**, 652 (2003).
[36] G. Batchelor, *The Theory of Homogeneous Turbulence* (Cambridge University Press, Cambridge, 1953).

[37] N. Fogla, F. Creta, and M. Matalon, Combust. Flame (2016), doi:10.1016/j.combustflame.2016.06.023.
[38] P. Pelce and P. Clavin, J. Fluid Mech. **124**, 219 (1982).
[39] M. Frankel and G. Sivashinsky, Combust. Sci. Technol. **29**, 207 (1982).
[40] F. Creta and M. Matalon, Proc. Comb. Inst. **33**, 1087 (2011).
[41] G. Giannakopoulos, A. Gatzoulis, C. E. Frouzakis, M. Matalon, and A. G. Tomboulides, Combust. Flame **162**, 1249 (2015).
[42] N. Chakraborty and S. Cant, Phys. Fluids **17**, 105105 (2005).
[43] D. Michelson and G. Sivashinsky, Acta Astronaut. **4**, 1207 (1977).
[44] O. Thual, U. Frisch, and M. Henon, J. Physique **46**, 1485 (1985).
[45] D. Vaynblat and M. Matalon, SIAM Journal on Applied Mathematics **60**, 679 (2000).
[46] V. Bychkov and M. Liberman, Phys. Rep. **325**, 115 (2000).
[47] G. Sivashinsky, Acta Astronaut. **4**, 1177 (1977).
[48] V. Bychkov, Phys. Fluids **10**, 2091 (1998).
[49] A. Lipatnikov, J. Chomiak, V. Sabelnikov, S. Nishiki, and T. Hasegawa, Proceedings of the Combustion Institute **35**, 1401 (2015).
[50] J. Driscoll, Prog. Energy Combust. Sci. **34**, 91 (2008).
[51] L. K. Tseng, M. A. Ismail, and G. M. Faeth, Combust. Flame **95**, 410 (1993).
[52] J. Bechtold and M. Matalon, Combust. Flame **127**, 1906 (2001).
[53] P. Clavin and P. Garcia, J. de Mechanique Theòrique et Appliqueè. **2**, 245 (1983).
[54] F. Picano, F. Battista, G. Troiani, and C. M. Casciola, Exp. Fluids **50**, 75 (2011).
[55] G. Troiani, M. Marrocco, S. Giammartini, and C. M. Casciola, Combust. Flame **156**, 608 (2009).
[56] G. Troiani, Combust. Flame **156**, 539 (2009).
[57] L. Kostiuk and R. Cheng, Combust. Flame **103**, 27 (1995).